

THE FLORIDA STATE UNIVERSITY

COLLEGE OF ARTS AND SCIENCES

**MUTATIONS IN THE HUMAN CARDIAC Ca^{2+} -REGULATORY
PROTEINS AFFECT THE FUNCTION OF THE THIN FILAMENT –
LESSONS FOR INHERITED CARDIOMYOPATHIES.**

By

NICOLAS BRUNET

A Dissertation submitted to the
Program in Molecular Biophysics
in partial fulfillment of the
requirements for the degree of
Doctor of Philosophy

Degree Awarded:
Fall Semester, 2006

The members of the Committee approve the Dissertation of Nicolas Brunet defended on October 25th, 2006.

P. Bryant Chase
Professor Directing Dissertation

Peng Xiong
Outside Committee Member

Timothy S. Moerland
Committee Member

Peter G. Fajer
Committee Member

Thomas C. S. Keller III
Committee Member

Approved:

Timothy Logan, Director, Institute of Molecular Biophysics

The Office of Graduate Studies has verified and approved the above named committee members.

This dissertation is dedicated with loving appreciation to my wife, Rosario Malpica, and my two children, Ethan and Rubi.

ACKNOWLEDGEMENTS

I would like to thank my major professor and advisor, Dr. P. Bryant Chase, for his guidance, expertise, encouragements, support, and patience throughout my graduate study.

I would also like to thank my committee members, Dr. Peng Xiong, Dr. Timothy S. Moerland, Peter G. Fajer, and Dr. Thomas C. S. Keller III, for their support and guidance.

Many persons helped me out during my research. They increased my insight in scientific research, helped me to expand my skills, or simply offered me a helping hand while conducting experiments. Therefore I am grateful to Dianne Taylor, Dr. Kim Riddle, Thomas Fellers, Dr. Steve Miller, Dr. Margaret Seavy, Rani Dhanarajan, Dr. Goran Mihajlović, Dr. Stephan von Molnár, Dr. Fang Wang, Dr. Brenda Schoffstall, Shanedah Williams, Lori McFadden, Aya Kataoka, Khaled Aledealat, Belinda Gavino, Lisa Compton, Vic Miller, Alyson Barnes and Neikeisha Sweeney.

Finally, I want to thank the Molecular Biophysics Graduate Program and the American Heart Association FL/PR Affiliate (0315097B) for funding my research.

TABLE OF CONTENTS

List of Tables	Page vii
List of Figures	Page viii
List of Abbreviations	Page xi
Abstract	Page xv
1. Introduction	Page 1
1.1 The Cross-Bridge Cycle and Thin Filament Regulation.....	Page 2
1.2 Effects of Temperature on Muscle Function	Page 3
1.3 The Structure of the Thin Filaments	Page 4
1.4 FHC Mutants.....	Page 8
1.4 In Vitro Motility.....	Page 9
2. Methods	Page 11
2.1 Protein Preparation.....	Page 11
2.1.1 Rabbit Skeletal Actin, Rabbit Skeletal Myosin and HMM, and Porcine Cardiac Myosin.....	Page 11
2.1.2 Human Tropomyosin and Mutants	Page 12
2.1.3 Human Cardiac Troponin and Mutants.....	Page 13
2.2 In Vitro Motility Assays	Page 23
2.2.1 Solutions	Page 23
2.2.2 Flow Cell Preparation	Page 26
2.2.3 Temperature Transients	Page 27
2.2.4 Data Acquisition and Analysis.....	Page 30
2.2.5 HMM Density (ρ).....	Page 30
2.2.6 Calculation of Speed, pCa_{50} , and HMM Duty Ratio (f)	Page 32
2.3 Statistical Analyses	Page 34
3. Results	Page 35
3.1 The Study of Human Cardiac Contractility in Vitro.....	Page 35
3.1.1 Functionality of Expressed Recombinant Human Tropomyosin.	Page 35
3.1.2 Characterization of the Co-expressed Recombinant Human Cardiac Troponin Complex.....	Page 35
3.1.3 Effects of MHC Isoform on Regulated Thin Filament Sliding....	Page 36
3.2 Temperature Dependence of Filament Sliding Speed	Page 41
3.2.1 Probing the Temperature Sensitivity of Sliding Speed in the <i>In Vitro Motility</i> Assay with a Microscopic Thermo-electric Heater.	Page 41
3.2.2 Temperature Dependence of Unregulated Actin and Regulated Thin Filament Sliding.....	Page 44

3.3 Dependence of Sliding Speed on Motor Density and Filament Length at 30°C	Page 48
3.4 Kinetic Basis for Biphasic Arrhenius Plots	Page 53
3.5 Effects of Metabolite Concentration on Temperature Sensitivity of Filament Sliding.....	Page 55
3.5.1 Reduced HMM Density	Page 55
3.5.2 Perturbation of ATP, ADP and Pi Concentrations.....	Page 56
3.6 Characterization of FHC Mutations in hcTn and α Tm.....	Page 63
3.6.1 The Effect of FHC Mutations in hcTn on Ca ²⁺ Sensitivity at 30°C	Page 64
3.6.2 Effect of FHC Mutations in hcTn on the Dependence of Sliding Speed on Motor Density at 30°C and at pCa 5	Page 67
3.6.3 Effect of FHC Mutations on the Thermal Stability and Temperature Dependence of Thin Filament Sliding.....	Page 71
3.6.4 Do FHC Mutations Affect the Cross-Bridge Duty Ratio During Unloaded Filament Sliding?	Page 74
4. Discussion	Page 76
4.1 Ca ²⁺ -Sensitivity of Human Cardiac Thin Filament Sliding Does not Depend Upon MHC Isoform	Page 77
4.2 Co-expression and Purification of the Three Subunits of Recombinant Human Cardiac Troponin	Page 78
4.3 Functional Assays for Thermal Stability of Regulated Actin.....	Page 79
4.4 Tn-Tm Enhancement of Maximum Filament Sliding Speed.....	Page 80
4.5 Do Factors that Limit Sliding Speed Change with Temperature?	Page 80
4.6 Effect of FHC Mutations on the Thermal Stability, Cross-Bridge Dependent Activation and the Calcium Sensitivity of Thin Filaments	Page 84
4.7 Troponin Structure: Lessons Learned from Single and Double Mutants.....	Page 86
5. Future Directions	Page 89
5.1 Do Cardiac Troponin and Myosin Interact with Each Other?	Page 89
APPENDIX	Page 93
REFERENCES	Page 95
BIOGRAPHICAL SKETCH	Page 108

LIST OF TABLES

Table 2.1: Metabolite concentrations in motility buffers.....	Page 25
Table 3.1: Activation energy for sliding speed calculated over the temperature ranges 27 – 32°C and 37 – 42°C from the data in Figs. 4 – 6	Page 57
Table 3.2: Motility speed-pCa regression parameter estimates for regulated F-actin containing α TM and WT or mutant hcTn	Page 66
Table 3.3: Motility speed- ρ regression parameter estimates for regulated F-actin containing either native hcTn and WT or mutant α TM or recombinant WT or mutant hcTn and α Tm.....	Page 69

LIST OF FIGURES

Figure 1.1: Schematic representation of the interactions between the thin filament components	Page 6
Figure 1.2: Schematic presentation of the conformation of Tn in the apo and the Ca ²⁺ state	Page 7
Figure 2.1: SDS-PAGE showing purification steps of bacterial expressed WT α Tm at various steps of purification	Page 14
Figure 2.2: Bacterial co-expression vector of recombinant human cardiac troponin (rhcTn) complex	Page 15
Figure 2.3: SDS-PAGE analysis of the bacterially co-expressed rhcTn complex	Page 18
Figure 2.4: Separation of the troponin complex from GST and TEV by anion exchange chromatography	Page 19
Figure 2.5: Western blot analysis of the co-expressed rhcTn complex	Page 20
Figure 2.6: Separation of the subunits of rhcTn by reverse phase HPLC.....	Page 21
Figure 2.7: SDS-PAGE analysis of representative protein preparations for rhcTn WT and mutants used in this study	Page 24
Figure 2.8: Design and calibration of the thermo-electric controller for motility assays	Page 28
Figure 2.9: Schematic of motility surface of flow cell modified with Au heating elements and electrically insulated with a 100 nm layer of SiO ₂ and fluorescence images (30 frames; 5 seconds) of motile F-actin	Page 29
Figure 2.10: Analysis of actin motility	Page 31
Figure 3.1: TEM micrographs of negatively stained F-actin- α Tm-EGTA and F-actin- α Tm-rhcTn-EGTA complexes on positively charged lipid monolayers	Page 37
Figure 3.2: Effect of recombinant human cardiac regulatory protein concentration on motility at pCa 9 and pCa 5	Page 38
Figure 3.3: Ca ²⁺ -sensitivity of sliding speed for regulated thin filaments propelled by pcMyosin or rsHMM	Page 40

Figure 3.4: Actin filament sliding speed response as a function of time upon cyclical heating and cooling for three cycles	Page 42
Figure 3.5: Speed of actin filaments as a function of temperature obtained from heating phases of the three cycles shown in Fig. 3.4	Page 43
Figure 3.6: Response in actin filament speed as a function of time upon rapid (< 1 s) temperature increase	Page 45
Figure 3.7: Temperature dependence of filament sliding speed in flow cells configured with a micro-fabricated thermo-electric heater	Page 47
Figure 3.8: Variation of ρ with [HMM] infused into flow cells, determined by K-EDTA ATPase assays	Page 49
Figure 3.9: Dependence of sliding speed on filament length for regulated and unregulated actin filaments at low or high surface densities of HMM at pCa 5 and 30°C	Page 50
Figure 3.10: HMM density (ρ) dependence of duty ratio (f) assuming the nearest neighbor model (Eq. 5) or the band model (Eq. 4) and (C) $\eta(\rho) \times s_m$	Page 52
Figure 3.11: Temperature dependence of two apparent rate constants that may limit sliding speed for regulated versus unregulated thin filaments	Page 54
Figure 3.12: Temperature dependence of sliding speed for unregulated actin and regulated thin filaments reconstituted with native hcTn and α Tm when [ADP] and [Pi] were reduced	Page 58
Figure 3.13: Temperature dependence of motility for unregulated actin and actin regulated with native hcTn and α Tm when surface density of HMM was reduced	Page 60
Figure 3.14: Temperature dependence of sliding speed for unregulated actin and regulated thin filaments reconstituted with native hcTn and α Tm when [ATP] was reduced, [Pi] was increased, or [ADP] was increased relative to control	Page 62
Figure 3.15: Effect of FHC hcTn mutations on the calcium-sensitivity of thin filament sliding at 30°C and pCa 5	Page 65
Figure 3.16: Effect of FHC hcTn (A) or α Tm (B) mutations on the ρ -dependency of thin filaments sliding speed at 30°C and pCa 5	Page 68

Figure 3.17: Loss of thin filament regulation at high temperature, shown by comparing sliding speeds of regulated thin filament speed – at low and high Ca^{2+} – with unregulated actin over a broad range of temperatures	Page 70
Figure 3.18: Temperature dependence of the sliding speed of thin filaments reconstituted with cardiac regulatory proteins bearing FHC-linked mutations	Page 72
Figure 3.19: Arrhenius analysis of the effect of FHC mutations in hcTn on the filament sliding speed.....	Page 73
Figure 3.20: Cross-bridge duty ratio (f) during unloaded filament sliding of regulated thin filaments	Page 75
Figure 4.1: Correction for temperature dependent effects of solvent viscosity on filament sliding speed of regulated and unregulated actin filaments	Page 82
Figure 4.2: Effect of the FHC mutations TnI R145 G and TnT R278C on the secondary structure, as predicted by GOR IV	Page 87
Figure 5.1: In vitro motility assays of unregulated F-actin, actin reconstituted with either rhcTn or α Tm alone, and actin regulated with both hcTn and α Tm at 30°C	Page 91
Figure 5.2: Pi production by MgATP hydrolysis for HMM in solution with or without addition of rhcTn	Page 92

LIST OF ABBREVIATIONS

%	Percentage
°C	Degrees Celcius
α Tm	Alpha Tropomyosin
β Tm	Beta Tropomyosin
ρ	Density of HMM on the NC-coated Surface
ADP	Adenosine Diphosphate
ATP	Adenosine Triphosphate
Ca ²⁺	Calcium
CK	Creatine Kinase
CP	Creatine Phosphate
Cr	Creatine
cTn	Cardiac Troponin Complex
cTnC	Cardiac Troponin C
cTnI	Cardiac Troponin I

cTnT	Cardiac Troponin T
d	Distance
DSC	Differential Scanning Calorimetry
d_x	Myosin Step Size
E_a	Activation Energy
f	HMM Duty Ratio
F-actin	Filamentous actin
FHC	Familial Hypertrophic Cardiomyopathy
HCM	Hypertrophic Cardiomyopathy
hcTn	Human Cardiac Troponin Complex
HMM	Heavy Meromyosin
HPLC	High Performance Liquid Chromatography
IVM	In Vitro Motility
l	Actin Filament Length
MB	Motility Buffer
MBP	Maltose-binding Protein

MS	Mass Spectrometry
n	The Hill Coefficient
N	The Number of Potential Cross-bridges
NC	Nitrocellulose
PcMyosin	Porcine Cardiac Myosin
Pi	Inorganic Phosphate
rhcTn	Recombinant Human Cardiac Troponin Complex
RhPh	Rhodamine Phalloidin
RP	Reversed Phase
S1	Myosin Subfragment 1
SPR	Surface Plasmon Resonance
s	Filament Sliding Speed
s_o	Filament Sliding Speed at Low Ca^{2+}
s_m	Maximum Sliding Speed
T	Temperature

TEV	Tobacco Etch Virus
Tm	Tropomyosin
Tn	Troponin Complex
TnT1	N-terminal domain of Troponin
TnT2	C-terminal domain of Troponin
t_s	Duration of Cross-bridge Attachment
T_t	Transition Temperature

ABSTRACT

Familial hypertrophic cardiomyopathy (FHC) is the leading cause of sudden cardiac death in both preadolescents and adolescents. The hallmark of the disorder is myocardial hypertrophy of the left ventricle, which results in an obstruction of blood flow through the left ventricular outflow tract. FHC has been associated with well over 100 mutations, primarily in proteins of the contractile apparatus of the heart. The molecular mechanisms involved in the pathogenesis of FHC are not well understood. For this study, *in vitro motility* assays (IVM) were conducted to assess the relationship between structure and function of cardiac thin filaments and to elucidate the molecular basis for sequelae of FHC caused by point mutations in the human cardiac regulatory proteins. Our research aims to contribute to the study of FHC by the accomplishment of the following innovations:

- 1) Development of a simple strategy to express recombinant human cardiac regulatory proteins in *E. coli* for molecular assays of human cardiac contractility.
- 2) Fabrication of a thermo-electric controller that allows rapid and reversible characterization over a broad temperature range of the effects of FHC mutations in troponin and tropomyosin using IVM assays.

My research yielded the following novel physiological findings

- 1) Ca^{2+} -sensitivity of human cardiac thin filament sliding is affected by some of the FHC mutations in the cardiac regulatory proteins, but not by changes in myosin isoform, indicating that Ca^{2+} -sensitivity does not depend upon the kinetics of cross-bridge cycling. This finding implies that the hypertrophic response is communicated through different pathways depending whether the mutation is in troponin, tropomyosin, or myosin
- 2) Troponin and tropomyosin affect the temperature sensitivity as well as the maximum speed of unloaded filament sliding by reducing the myosin cross-bridge duty ratio. Our results suggest that the duty ratio also might be affected by clinically relevant mutations in troponin and tropomyosin.

Finally, functional characterization of troponin, bearing FHC mutations in subunit I, subunit T, or both subunits, predicts structural relationships of the thin filament.

CHAPTER 1

INTRODUCTION

Hypertrophic cardiomyopathy (HCM), formally described in 1952 [1] is a disease of heart muscle and associated with cardiac dysfunction. HCM is characterized by an increase of the left ventricular wall thickness due to myocyte hypertrophy, myofibrillar disarray, and interstitial fibrosis. Approximately two-thirds of the patients have a family history of HCM. Familial HCM, the hereditary form of HCM or familial hypertrophic cardiomyopathy (FHC), is one of the most common cardiac disorders with prevalence in young adults of one in 500. Most, but not all, FHC-linked disease-causing genes encode protein components of the cardiac sarcomere. Mutations in the β myosin heavy chain account for $\sim 35\%$ of all FHC cases, followed by mutations in the Myosin binding protein C ($\sim 20\%$), cardiac troponin T (cTnT; $\sim 20\%$), α -tropomyosin (α Tm $\sim 5\%$), and cardiac troponin I (cTnI; $\sim 5\%$). Mutations in the essential and regulatory myosin light chains, cardiac α -actin, titin and others have been reported but are relatively rare. A strikingly high frequency of early sudden cardiac death has been reported for patients carrying mutations in the cardiac regulatory proteins [2-4]; clinical presentation of FHC mutations in α Tm, cTnI and cTnT are often distinct and complex with varying degrees of ventricular hypertrophy. Data from genotype-phenotype correlated studies, limited by the small number of kindred studies and family sizes available for analysis, shows that the clinical phenotype also varies between individuals with the same mutation. Although large numbers of specific mutations that are causal of cardiomyopathies have been identified, the functional consequences of gene mutations and precise details of the signaling pathways that lead to hypertrophy remain to be elucidated.

This study aims to provide new insights in how cardiac regulatory proteins Tn and Tm regulate unloaded thin filament sliding, how regulation is affected by mutations in α Tm, cTnI and cTnT, and how the study of FHC mutations can contribute to our knowledge of the thin filament structure.

Our current understanding of the molecular basis of muscle contraction with emphasis placed on features relevant to this study such as temperature effects, thin filament structure and

clinically relevant mutations, is briefly summarized in this chapter. The use of *in vitro motility* assays (IVM), the principal technique used for this study, is also addressed.

1.1 The Cross-Bridge Cycle and Thin Filament Regulation.

Muscle contraction occurs when actin and myosin filaments slide past each other, driven by myosin heads walking towards the plus end of the adjacent actin filament in a process that is mediated by the cyclical attachment and detachment of cross-bridges. During one cross-bridge cycle actin combines with myosin and adenosine triphosphate (ATP) to produce force, adenosine diphosphate (ADP) and inorganic phosphate (P_i). Calcium regulation of the cross-bridge cycle in vertebrate striated muscle is mediated by the troponin complex (Tn) and tropomyosin (Tm). The most recent scientific contributions to our understanding of the cross-bridge cycle and its regulation are provided by data from structural, biochemical, physiological and *in vitro* motility studies and have been summarized by Gordon *et al.* [5]. The steric blocking model of Ca^{2+} -regulation originally predicted that Tm moves reversibly from a position that prevents strong binding to a position that allows strong binding of myosin to actin upon Ca^{2+} binding. Based on X-ray diffraction, EM reconstruction studies [6-9], and confirmed by biochemical evidence [10], this model has been extended to a three-state dynamic steric hypothesis. The three-state model postulates that in the off position Tm only allows weak electrostatic actomyosin interactions [6, 7] (blocked position). After Ca^{2+} -binding to troponin, Tn moves $\sim 25^\circ$ [6, 8, 9] and exposes additional binding sites, promoting stronger hydrophobic binding of actin to myosin (closed state), but upon the addition of myosin cross-bridges Tm moves another 10° [8] around the actin filaments, exposing even more of the myosin binding sites (open state).

The role ascribed to thin filament Ca^{2+} -regulatory proteins tropomyosin (Tm) and troponin (Tn) is, however, suspected to be more than a simple calcium switch because, in motility assays, regulatory proteins in many instances enhance the maximum sliding speed at high Ca^{2+} over that obtained with unregulated actin [11-17]. In skinned fibers, the maximum isometric tension per cross-bridge is 50% – 70% greater in the presence of regulatory proteins [18, 19], and can be even larger in single thin filaments [14, 17, 20]. Actomyosin function might be enhanced because Tm and Tn modulate the fraction of the cross-bridge cycle that myosin spends in a strong-binding state (f ; duty ratio). If true, f might be Tn/Tm isoform specific and

even be affected by mutations in FHC that have been reported to decrease or increase maximum unloaded sliding speed with respect to WT (references). Subtle changes in T_m and/or T_n might change the actin- T_m interface, modifying the rate of actomyosin association and disassociation and/or the time of the power stroke. The absence of T_m/T_n would expose the actin-myosin binding sites completely and therefore permitting the strongest possible interaction, resulting in a slow disassociation and finally a slower motility for unregulated versus regulated actin. A change in f , mediated by the $T_m \cdot T_n$ complex, and sensitive to some of the FHC-mutants, could alternatively be explained by a tropomyosin-induced conformational change of actin [21, 22].

By exploring the dependency of unloaded sliding speed on HMM density and filament length for both unregulated actin and regulated thin filaments at saturating Ca^{2+} (pCa 5), we could demonstrate that f for regulated thin filaments was lower than unregulated actin at all HMM densities tested. Revealing the molecular mechanisms leading to a change in f were beyond the scope of this study, but will be considered (see Future directions).

1.2 Effects of Temperature on Muscle Function.

Effects of $T_n \cdot T_m$ on muscle function vary markedly as temperature approaches physiological levels [16, 17, 23]. Temperature is an important determinant of mammalian striated muscle contraction. The influence of temperature on muscle function appears to be greater at low temperatures often used experimentally than at physiological temperatures; examples are isometric tetanic tension [24-26] and maximum mechanical power output [27]. Temperature modulates the control of striated muscle contraction by the Ca^{2+} regulatory proteins $T_n \cdot T_m$, although there are both qualitative and quantitative discrepancies on these effects in the skeletal muscle literature [25, 28, 29]. Counterintuitively, mild hypothermia has been reported to be a positive inotropic effector in living cardiac muscle due to interplay between temperature and cardiac thin filament Ca^{2+} regulation [30].

The temperature dependence of unloaded filament sliding speed has been reported to change as a function of temperature [16, 31, 32]. For unregulated actin, Arrhenius plots have been reported to be linear within 20 – 60°C (Fig. 3C) [33] and 7 – 25°C [16], but non-linear within 3 – 42°C with a transition temperature (T_i) of 15.4°C [31], and 10 – 35°C with a $T_i \sim 25^\circ C$ [32, 34]. Given the differences in experimental temperature ranges, these results suggest there

exists at least one T_t that might be sensitive to experimental conditions. For regulated thin filaments, Homsher et al. [16] observed a break in the Arrhenius plot around 12.5°C that was not seen for unregulated actin within the 7 – 25°C temperature range, indicating that the T_t in the Arrhenius plot may also depend on whether or not actin is regulated. In support of this hypothesis, the Arrhenius plot of fish myofibrillar ATPase at saturating Ca^{2+} exhibited a breakpoint [35], while this was not the case for in vitro motility sliding speed and actin-activated MgATPase activity with fish myosin and unregulated F-actin [36]. Thus, from the limited data available, it is not known if—in addition to enhancing actomyosin function—Tn·Tm modulates the temperature-dependence of unloaded filament sliding around physiological temperatures for mammalian species, and for human cardiac Tn·Tm in particular.

To study the possible modulatory role of Tn·Tm in the temperature sensitivity of cardiac muscle function, we studied the effect of temperature on the speed of F-actin with and without human cardiac Tn and Tm at pCa 5 over a broad temperature range (~ 20 – 60°C) using a thermo-electric controller [33]. Arrhenius plots were non-linear for regulated but not unregulated actin. One explanation is that regulated sliding speed is limited by discontinuous sliding at low temperature ($T < \sim 38^\circ\text{C}$). At high temperature ($T > \sim 38^\circ\text{C}$), in contrast, speed may be limited by the duration of the stroking time (t_s). In addition, our results suggest that t_s for unregulated sliding is greater than for regulated thin filament sliding. Therefore our model predicts that the T_t at which continuous sliding is achieved for unregulated actin occurs below the temperature range of our assay, consistent with previous reports [31, 32]. Changes in sliding speed and temperature-sensitivity when concentrations of ATP or Pi were altered, or HMM density was changed, were consistent with predictions of our model.

1.3 The Structure of the Thin Filaments.

Tn and Tm are located along polymerized actin at a Tn:Tm ratio of 1:1 [37]. A structural regulatory unit of the thin filament is composed of one molecule of Tm, one Tn complex, and seven actin monomers [5, 38]. Tm, first discovered by Bailey [39] is an extended parallel α -helical coiled-coil dimer. Adjacent Tm's interact in a head-to-tail fashion to form continuous strands along the actin helix, with two such strands on opposite sides of a thin filament [40, 41]. Tn contains three subunits: calmodulin-like TnC binds Ca^{2+} ; TnI inhibits the actomyosin ATPase

at low calcium; and TnT anchors Tn to Tm. Each Tm/Tn complex spans and regulates seven actin monomers. The Tn complex is anchored to Tm through the Ca^{2+} -insensitive, extended N-terminal domain of TnT (TnT1), whereas the C-terminus of TnT (TnT2) forms the globular core domain with TnI and TnC [42-47]. The mechanism by which changes in the interaction between TnC and TnI, induced by reversible binding of Ca^{2+} to TnC, ultimately leads to an azimuthal shift of tropomyosin on actin is only partly understood. In 2003, Takeda and co-workers presented a high-resolution crystal structure of the core domain in the Ca^{2+} -saturated form [44]. A diagram (Fig. 1.1), created by Takeda et al. [44] expresses the current understanding of the interaction between troponin and the other thin filament components: Cardiac muscle contraction is initiated by the binding of Ca^{2+} to site II, the only active helix-loop-helix EF-hand metal-binding motif in the N-terminal domain (site I, also situated in the N-terminal domain is inactive while sites III and IV, located in the C-terminal domain are occupied with Mg^{2+} under physiological conditions). The N-lobe then undergoes a structural transition from a closed to an open form, priming a hydrophobic patch of the N-terminal region (see Gagné et al. [48] and McKay et al. [49] for the skeletal variant) for binding of the helix H3 of TnI, also called the switch domain (cTnI 147-163). The TnI-TnC binding event likely promotes a rotation of the IT arm, which consist of a rigid α -helical coiled-coil formed between portions of TnT (cTnT 226-271) and TnI (cTnI 90-136) as observed in the Takeda structure (Fig. 1.1) and predicted previously [50, 51]. Rotation of the IT arm, driven by the calcium-induced TnI-TnC interaction causes the release of the TnI inhibitory region (cTnI 128-147 and the TnI mobile domain (cTnI 164-210) from actin-tropomyosin so that Tn is only anchored to the thin filament through the Ca^{2+} -insensitive TnT1.

Properties and function of tropomyosin have been broadly reviewed by Perry [45]. Tm consists of two α -helical polypeptide chains, intertwined with each other into a stable coiled-coil structure. The polypeptide chain of each Tm subunit consists of seven regions, each exhibiting a similar amino acid composition and actin interaction sites. Tm is polymerized into filaments along actin by an 8-9 amino acid residue overlap between the N- and C-termini [52, 53]. Lehrer and co-workers [54, 55] showed that unfolded mixtures of α - and β -isoform of *Rana esculenta* skeletal or duck gizzard Tm preferentially reassembled as $\alpha\alpha$ or $\beta\beta$ homodimers at 20°C,

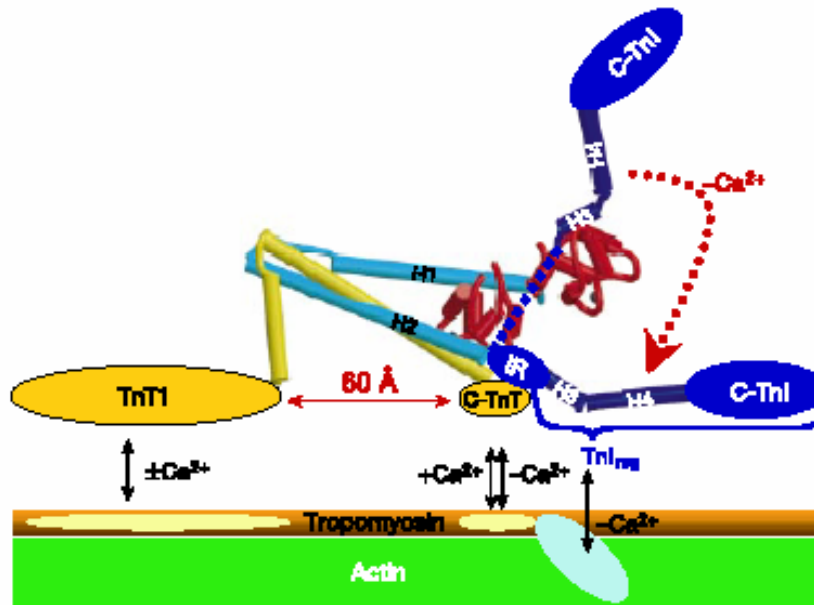


Figure 1.1: Schematic representation of the interactions between the thin filament components. Components are TnT (yellow), TnC (red), TnI (blue), Tropomyosin (brown) and actin (green). Figure from Takeda et al. [44]. The black arrows indicate the interaction between troponin and tropomyosin-actin.

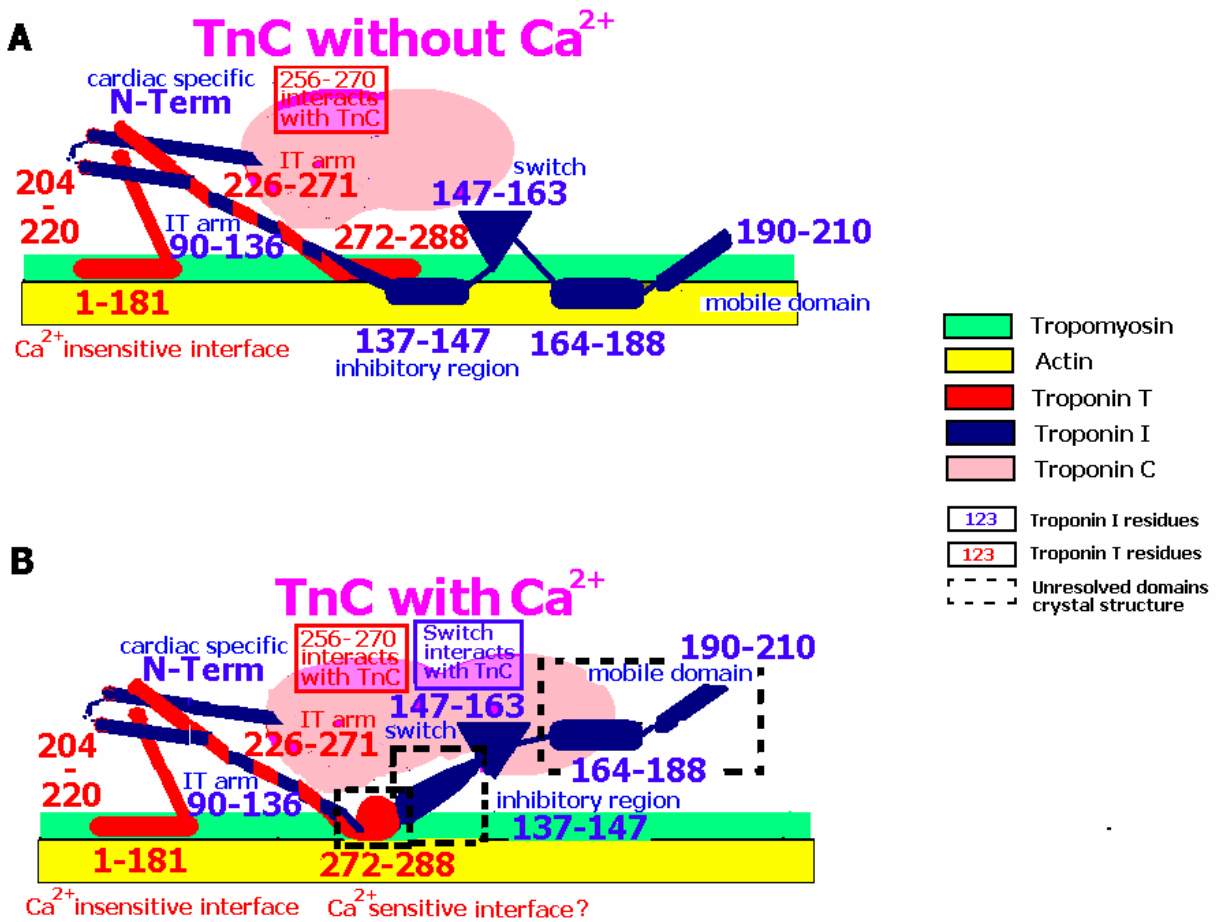


Figure 1.2: Schematic presentation of the conformation of Tn in the (A) apo and the (B) Ca²⁺ state. Regions TnT 272-288, TnI 147-163 and TnI 164-210 (dotted boxes) are not resolved in crystal structures of Tn.

and as $\alpha\beta$ heterodimers at physiological temperature, suggesting that Tm is a very dynamic structure and consistent with reports that Tm is a very flexible dimer [56-59].

1.4 FHC Mutants.

Crystallization trials of the whole troponin complex have been unsuccessful thus far. The most complete picture of the core domain of hcTn in the Ca^{2+} saturated form was elaborated by Takeda and co-workers [44]; they managed to crystallize a complex consisting of TnC(1-161), TnI(31-210) and TnT(183-288), which yielded a high quality structure. Regions associated with calcium dependent actin and tropomyosin interfaces [43, 44], however, were ambiguous and could not be resolved. They include the TnI inhibitory region (TnI 137-148), the TnI C-terminus (TnI 163-210) and the TnT C-terminus (TnT 272-288). It is possible that these regions do not fold properly in solution or that they contain flexible linkers that allow multiple conformations. It is perhaps not a coincidence that these regions are prone to FHC mutations. TnI regions 137-148 and 162-210 account for 20 out of 24 reported mutations in TnI [60]: R141Q, R145G, R145Q, R145W, R162Q, S166F, K178E, K183E, R162W, Kdel183, R162P, K177del, R186Q, D190G, R192H, D196N, S199G, G203R, G203S, K206Q. TnT region 272-288, despite being only 17 amino acids long, accounts for 7 out of 24 reported mutations [60] including N271I, K273E, R278C, R278P, R286H, R286C, and W287X (truncation). Knowledge regarding the structure of these FHC hotspots might be necessary for the identification of rational therapies that could help to alleviate the pathological symptoms associated with these mutations.

The three FHC mutations in hcTn selected for this study – TnI R145G, TnI K206Q, and TnT R278C – each correspond with one of the unresolved regions in the high Ca^{2+} hcTn structure (Fig. 1.2). Interestingly, if the coiled-coil of the IT arm would be 1.5 heptad repeats longer, then TnI R145 would be at an “a” position and TnT R278 at the paired “d” position (COILS 2 algorithm). To investigate if these two FHC mutations, downstream from the coiled-coil reside in the same vicinity, we also engineered an hcTnI bearing both the TnI R145G and the TnT R278C mutation.

Ten FHC mutations in Tm are listed in the Human mutation databases [60]. Mutants αTm D175N and αTm E180G were chosen for this study. Both mutations are in highly conserved parts of the Tm molecule and are situated in the region of the fifth actin binding site [61, 62].

Effects of α Tm D175N and α Tm E180G with respect to maximum force, maximum shortening velocity, calcium sensitivity, affinity for actin, Tm stability, Tm flexibility, and left ventricular performance have been reported [62-68]. The results varied very often, depending on the experimental system, methodology and source of proteins that were used and caution must be exercised in drawing conclusions from them [45]. Therefore, we used the *in vitro* motility assay to characterize α Tm D175N and α Tm E180G by exploring parameters that have not been reported before.

1.5 In Vitro Motility.

The *in vitro motility* (IVM) assay is the major technique applied in this study. By studying the relation between actin filament length and filament sliding speed while varying the concentration of competitive motor heads on the assay surface of a motility assay [69] we could estimate the duty ratio for unregulated actin and regulated thin filaments. The specificity with which chemical and genetically modified proteins can be substituted and correlated with effects on mechanical behavior made IVM assays a powerful tool [5, 70] to characterize the effect of cardiac troponin mutations that cause familial hypertrophic cardiomyopathy. One of the parameters, traditionally measured to compare function and performance of mutants versus wild type is the maximum filament sliding speed (s_m) and the other, obtained by varying $[Ca^{2+}]$, is the calcium sensitivity.

In addition, we used IVM technique to explore two more parameters that potentially could be affected by mutations in Tn and/or Tm: We investigated whether the number of motor heads on the surface required to achieve half maximum sliding speed changed when FHC mutations were incorporated into the thin filaments, and we also examined whether the thermal stability of the thin filament was affected by those mutants. The thermal stability of large ensembles of isolated proteins has classically been studied with techniques such as differential scanning calorimetry [71], light scattering experiments [72], and circular dichroism [73]. We were, however, able to construct a thermo-electric heater by modifying the classic cover slip that functions as the motility surface [33, 74] and monitor the sliding speed of thin filaments over a broad temperature range. This study might therefore, not only mark the beginning of a new application for an already powerful assay, but also promote the IVM assay as a suitable tool to

monitor the thermal effects on the function of protein complexes with quasi single-molecule sensitivity.

CHAPTER 2

METHODS

2.1 Protein Preparation.

2.1.1 Rabbit Skeletal Actin, Rabbit Skeletal Myosin and HMM, and Porcine Cardiac Myosin.

Myosin and the chymotryptic digest fragment heavy meromyosin (HMM) were prepared from fast skeletal muscle of adult male New Zealand White rabbits. All rabbits were handled in accordance with the current National Institutes of Health/National Research Council Guide for the Care and Use of Laboratory Animals. All procedures and protocols were approved by Florida State University's Institutional Animal Care and Use Committee. Rabbits were injected I.M. with 3 mg Acepromazine + 10 mg/kg Xylazine + 50 mg/kg Ketamine. Following verification of appropriate surgical depth of anesthesia, the rabbits were exsanguinated via laceration of the carotid artery. The euthanized animals were skinned, eviscerated, and chilled on ice. Back and leg muscles were removed for acetone powder, and back muscles only for myosin preparation [12, 75, 76].

HMM was made by chymotryptic digestion [77] from either freshly prepared myosin for experiments involving low HMM density, or from myosin stored < 5 weeks in glycerol (1:1) at -20°C for all other experiments; in both cases, HMM was used within three days after preparation.

Rabbit muscle actin was purified from back and leg muscle acetone powder by the method of Pardee and Spudich [78] as described previously [12, 75]. F-actin was labeled with rhodamine phalloidin (RhPh; Molecular Probes) for fluorescence microscopy. F-actin (33 µg/ml) and RhPh (1 µM) were incubated in AB with 1 mM DTT at 4°C overnight. This labeled F-actin solution was stable at 4°C for at least two weeks.

Porcine hearts were obtained from a local abattoir within 20 minutes of the animals' deaths. Porcine cardiac myosin (pcMyosin) was obtained from ventricular tissue using modifications of previously reported protocols for other species [79, 80]. ATP-insensitive "dead

heads” were removed from rabbit skeletal HMM (rsHMM) and pcMyosin preparations by ultracentrifugation in the presence of MgATP and F-actin on the day of use [77].

2.1.2 Human Tropomyosin and Mutants.

Full length human alpha tropomyosin (α Tm, accession no. M19713) and human beta tropomyosin (β Tm, accession no. X06825) cDNAs were amplified from a Marathon-Ready cDNA Library (CLONTECH Laboratories Inc., Palo Alto, CA, USA) made from human cardiac tissue by PCR with the designed primers. Both of the PCR products were then sequenced on an ABI 3100 Genetic Analyzer (Foster City, CA, USA) by using capillary electrophoresis and Version 2 Big Dye Terminators, as described by the manufacturer. The alignments of deduced amino acid sequences from both the PCR products and the published sequences (M19713 and X06825) were performed on Genetic Computer Group (GCG) software (Accelrys Inc., San Diego, USA) to confirm the sequence identities.

The cDNA inserts of both α Tm and β Tm were engineered with a BamHI site just before the start codon and a Sall site just after the stop codon by PCR using Pfu Turbu DNA polymerase (Stratagene Inc., Cedar Creek, TX, USA). The inserts were ligated to maltose-binding protein (MBP) fusion expression vector pMAL-c2 (New England BioLabs Inc., Beverly, MA, USA) in which a thrombin cleavage site has been engineered. DH₅ α cells were transformed with the ligation mixtures and the positive clones were identified by PCR with the same primers used in the cloning. The recombinant plasmids were extracted for expression and mutagenesis (α Tm only). Three α Tm mutants from clinical data, α TmV95A, D175N, and E180G, were generated by PCR using QuikChange XL Site-Directed Mutagenesis system (Stratagene). The reactions were carried out according to the manufacturer’s instruction with the template of α Tm/pMal-c2 plasmids and the following pairs of primers:

pTmV95Af: 5’-CGCATCCAGCTGGCTGAGGAAGAGTTGG-3’

pTmV95Ar: 5’-CCAACTCTTCCTCAGCCAGCTGGAACGTGC-3’

pTmD175Nf: 5’-GTCATCATTGAGAGCAACCTGGAACGTGC-3’

pTmD175Nr: 5’-GCACGTTCCAGGTTGCTCTCAATGATGACC-3’

pTmE180Gf: 5'-CGACCTGGAACGTGCAGGAGAGCGGGCTGAGCTCTC-3'

pTmE180Gr: 5'-GAGAGCTCAGCCCGCTCTCCTGCACGTTCCAGGTCG-3'

Plasmids extracted from three transformed mutants were sequenced with primers targeted at the flanks of MCS on pMAL-c2 vector to confirm sequence changes in the mutants. For expression, competent *E. coli* BL21 (DE₃) cells (Novagen Inc., Madison, WI, USA) were transformed with cDNA/pMal-c2 plasmids (α Tm, β Tm and three α Tm mutants). Single colonies were grown at 37°C to an OD₆₀₀ of 0.5, followed by induction with 0.3 mM IPTG. The cells were harvested, resuspended in amylose resin (New England BioLabs Inc.) column buffer (20 mM TrisCl, pH 7.4, 10 mM β -mercaptoethanol, 200 mM NaCl and 1 mM EDTA), lysed with mild sonication, centrifuged at 12,000g, passed over an amylose affinity column, and eluted with column buffer containing 10 mM maltose. Fusion proteins were cleaved with thrombin (Sigma, St. Louis, MO, USA) at one unit of thrombin per mg of protein in column buffer for four hours at room temperature. The liberated recombinant proteins were purified on a Mono Q column (Pharmacia Biotech, Uppsala, Sweden) by high performance liquid chromatography (HPLC) with a gradient elution (buffer A: 20 mM Tris·Cl, pH 8.0, 25 mM NaCl; buffer B: buffer A containing 500 mM NaCl). The BamHI site on pMAL-c2 vector is integral to the thrombin cleavage region so the recombinant Tm's all have two extra amino acids (GS-) at the N-terminal. GS- is a conservative alternative to the AS- dipeptide in bacterially expressed Tm that substitutes functionally for acetylation of Tm's N-terminus [81, 82]. The purified recombinant proteins were concentrated, aliquoted and stored at -80°C in HPLC elution buffer until use.

The purity of tropomyosin was determined by coomassie-stained Tricine-SDS PAGE [83] (Fig. 2.1). Gels were imaged using a Kodak EDAS 290 digital imaging system and quantified with Kodak 1D Image Analysis Software.

2.1.3 Human Cardiac Troponin and Mutants.

Two sources of human cardiac troponin (hcTn) were used for this study. The first source is purified native hcTn obtained from Research Diagnostics (Flanders, NJ, USA), and the second source was recombinant hcTn (rhcTn). The remainder of this section describes strategies employed to obtain highly purified, bacterially coexpressed rhcTn: Genes for hcTnT (P45379-6), hcTnI (P19429), and hcTnC (P63316) were cloned from a human heart cDNA library (BD

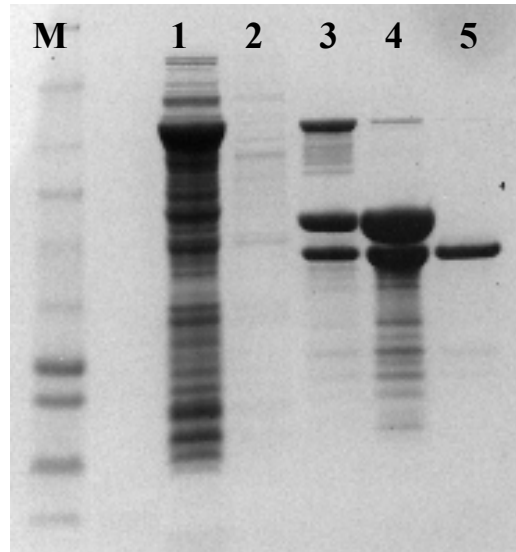


Figure 2.1: SDS-PAGE showing purification steps of bacterial expressed WT α Tm at various steps of purification. M: marker See Blue Plus MES (Invitrogen); 1: α Tm crude bacterial lysate; 2: Amylose affinity column void volume; 3: α Tm-MBP fusion protein after Amylose purification; 4: α Tm and MBP after thrombin protease cleavage; 5: α Tm after HPLC with a Mono Q anion exchange column (Uppsala, Sweden)

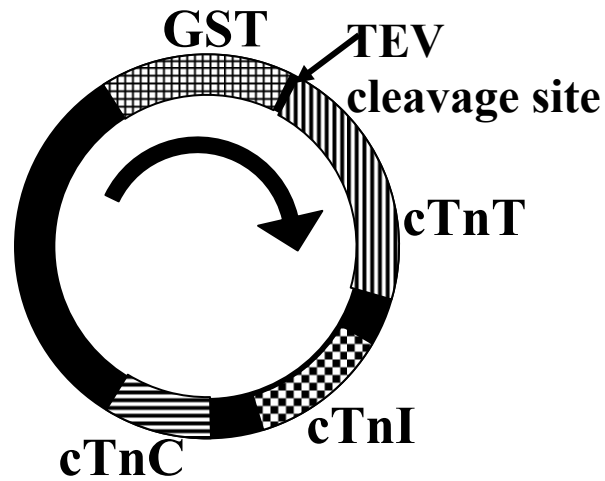


Figure 2.2: Bacterial co-expression vector of recombinant human cardiac troponin (rhcTn) complex. cDNA sequences for all three subunits of hcTn were cloned into pET 41a+ along with promoters and terminators for co-expression in *E. coli*. The plasmid was engineered with a GST tag at the N-terminus of hcTnT, and modified to include a TEV protease site between GST and hcTnT.

Biosciences Clontech, Palo Alto, CA) and individually ligated into the pET 11d vector (Novagen-EMD Biosciences, San Diego, CA). hcTnT was initially moved into the pET 41a+ vector (Novagen-EMD Biosciences, San Diego, CA) to create GST-hcTnT with the GST tag at the N-terminus and a TEV (Tobacco Etch Virus) protease cleavage site between GST and hcTnT. HcTnI and hcTnC, along with promoters and terminators, were sequentially moved into the same pET 41a+ vector along with hcTnT; the final plasmid contained the genes for all three subunits (Fig. 2.2). The sequence of the WT for all three subunits was in agreement with the listed Swiss-Prot accession numbers [43, 44]. A limited number of experiments (section 3.1), however, were conducted with troponin bearing mutation hcTnI D108G, which was spontaneously introduced during site-directed mutagenesis and discovered during the experimental phase of this study. cTnI D108 is located near the middle of the IT coiled-coil region and predicted to be at the "e" location (COILS algorithm). Analysis of the Ca²⁺ saturated core domain of cTn (structure PDB 1J1E) indicates that no ionic bond was interrupted upon introduction of the mutation. The mutation was corrected for all other experiments involving rhcTn.

To obtain a functional troponin complex, the above pET 41a+ hcTn expression plasmid containing all three subunits was transformed into BL21 STAR ultra-competent *E. coli* cells (Invitrogen Corp., Carlsbad, CA). Cultures were grown in 3 liters of LB broth (Sigma-Aldrich Co. St. Louis, MO) at 37°C until O.D. at 600 nm was 0.35-0.5, at which time protein expression was induced by addition of 0.4 mM IPTG. Four hours after induction, cells were harvested, pelleted by centrifugation, and frozen at -80°C. Frozen bacterial cell pellets were resuspended in GST Bind/Wash buffer (in mM: 4.3 Na₂HPO₄, 1.47 KH₂PO₄, 137 NaCl, and 2.7 KCl, pH 7.3) plus 2.5% streptomycin sulfate (Sigma), and then subjected to two rounds of rapid freeze-thaw. An additional 2.5% streptomycin sulfate was added to precipitate nucleic acids. The sample was centrifuged and the soluble crude bacterial lysate supernatant was dialyzed overnight against GST Bind/Wash buffer at 4°C.

GST-rhcTn was purified by affinity chromatography (BioLogic LP Chromatography System, BioRad, Hercules, CA, USA) using GST-Bind Resin (Novagen-EMD Biosciences, San Diego, CA, USA). GST-rhcTn was eluted with GST Elution Buffer (in mM: 50 Tris-HCl, pH 9.5 and 10 reduced glutathione). Fractions containing protein (monitored continuously at A₂₈₀) were pooled and protein concentration was determined using the Warburg-Christian method (DU 640

Spectrophotometer, Beckman Fullerton, CA, USA). The GST tag was cleaved from rhcTn by digestion with 50 Units AcTEV protease (Invitrogen) per mg fusion protein for 1.5 hours at room temperature. The cleaved sample was dialyzed overnight at 4°C against Tn dialysis and storage buffer (D&S buffer) composed of (in mM) 125 Imidazole-HCl, 125 KCl, 4 MgCl₂, and 2 CaCl₂. The TEV protease cleavage site was introduced for removal of the affinity tag because we found in preliminary studies that several other commonly used proteases promiscuously cleaved rhcTnT (data not shown). After removal of the GST tag, the N-terminus of rhcTnT was extended by only one additional amino acid, a glycine.

The GST tag and TEV protease were separated from rhcTn by anion exchange chromatography (DE52 resin, Whatman, Maidstone, UK). GST tag and TEV protease eluted in the void volume by washing the loaded column with D&S buffer (Fig. 2.3, 2.4). Purified rhcTn eluted in a single peak by applying a salt gradient of 125 mM KCl to 400 mM (Fig. 2.4). Fractions were analyzed by SDS-PAGE, and pure rhcTn fractions were pooled. The sample was concentrated using a 50,000 MWC Centricon filter device (Millipore Corp. Bedford, MA), and the concentration was determined as described above. Typical yield from three liters of culture was ~0.7 mg purified rhcTn. Aliquots were stored at -80°C, and used for *in vitro* motility within two weeks of preparation.

Coomassie-stained SDS-PAGE protein gels were imaged using an EDAS-290 digital imaging system (Kodak, Rochester, NY, USA) and band intensities were analyzed with ImageJ 1.34s (National Institutes of Health, USA). Purity was ~96 % (Fig. 2.3). Subunit stoichiometry was: rhcTnT, 0.99; rhcTnI, 0.90; and rhcTnC, 1.19 (expressed as % intensity rhcTn / % intensity purified human cTn complex, Research Diagnostics, Flanders, NJ, USA). Identity of the three subunits of rhcTn was confirmed by Western blot analysis (Fig. 2.5). Primary antibodies were: mouse anti-cardiac TnT, clone 1F11; mouse anti-cardiac TnC, clone 7B9; and mouse anti-cardiac TnI, clone 16A11 (Research Diagnostics, Flanders, NJ, USA) and secondary antibody was goat anti-mouse HRP conjugate (BioRad).

A Beckman System Gold HPLC (Beckman-Coulter, Fullerton, CA) equipped with a model 168 diode array detector, model 126 solvent delivery system and a Rheodyne 7125 sample injection valve was used for reversed phase (RP) chromatography. The rhcTn complex (50 µl of 0.26 µg/µl) was run on a Vydac C4 RP column (0.21 x 250 mm, The Nest Group, Southborough,

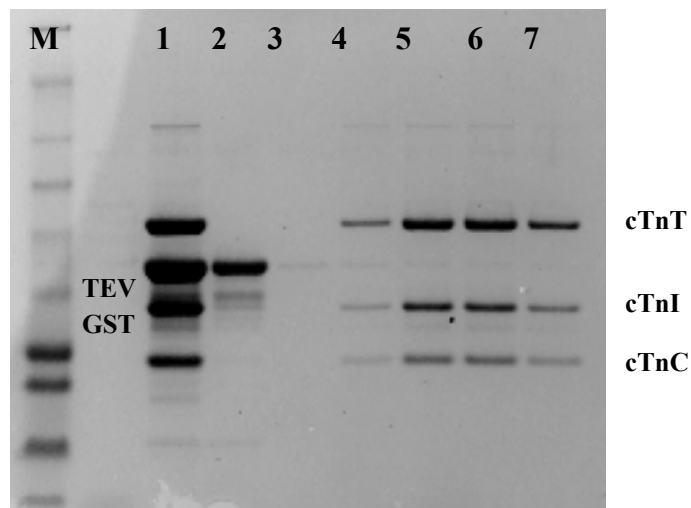


Figure 2.3: SDS-PAGE analysis of the bacterially co-expressed rhcTn complex. The protein complex, retained by GST affinity purification, yielded after removal of GST from the N-terminus of rhcTnT, all three desired subunits; densitometry analysis indicates ~96% purity. M: marker; 1: rhcTn complex after GST affinity purification and TEV protease cleavage; 2: Anion exchange chromatography (DE52) void volume, containing GST tag and TEV protease; 3-7: Anion exchange chromatography fractions eluted by salt gradient.

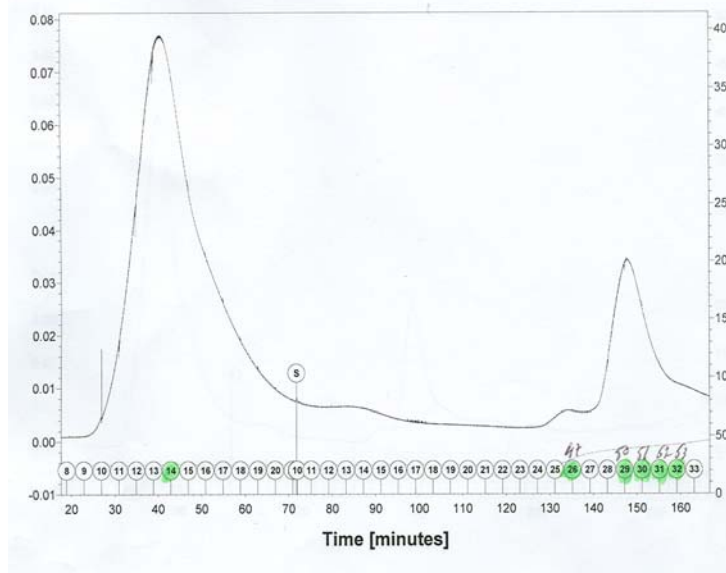


Figure 2.4: Separation of the troponin complex from GST and TEV by anion exchange chromatography. The GST tag and the TEV protease eluted first after washing the loaded column with a low salt buffer (first peak); subsequently, after applying a salt gradient, purified rhcTn eluted as a single peak (second peak).

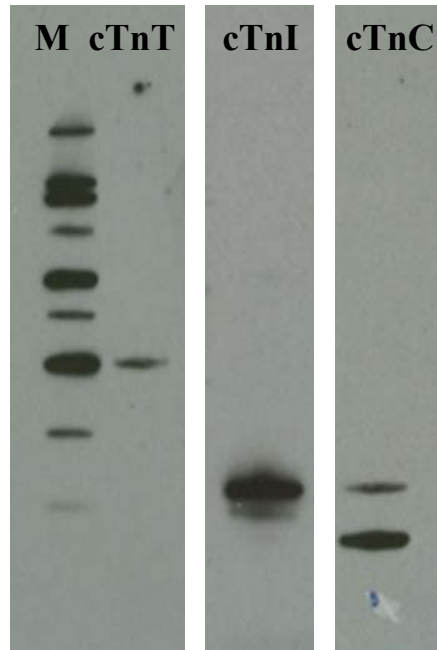


Figure 2.5: Western blot analysis of the co-expressed rhcTn complex. Specific antibodies for hcTnT (left), hcTnI (center), and hcTnC (right) detected bands of the appropriate sizes for each subunit (Methods). (M: marker). MagicMark XP Western Protein Standard (Invitrogen). The small band observed under cTnI might be the result of a cTnI degradation product, consistent with the results of the analysis of the band intensities from the SDS-Page protein gel indicating ~ 96% purity (Fig. 2.3). Analysis was performed by Lisa Compton.

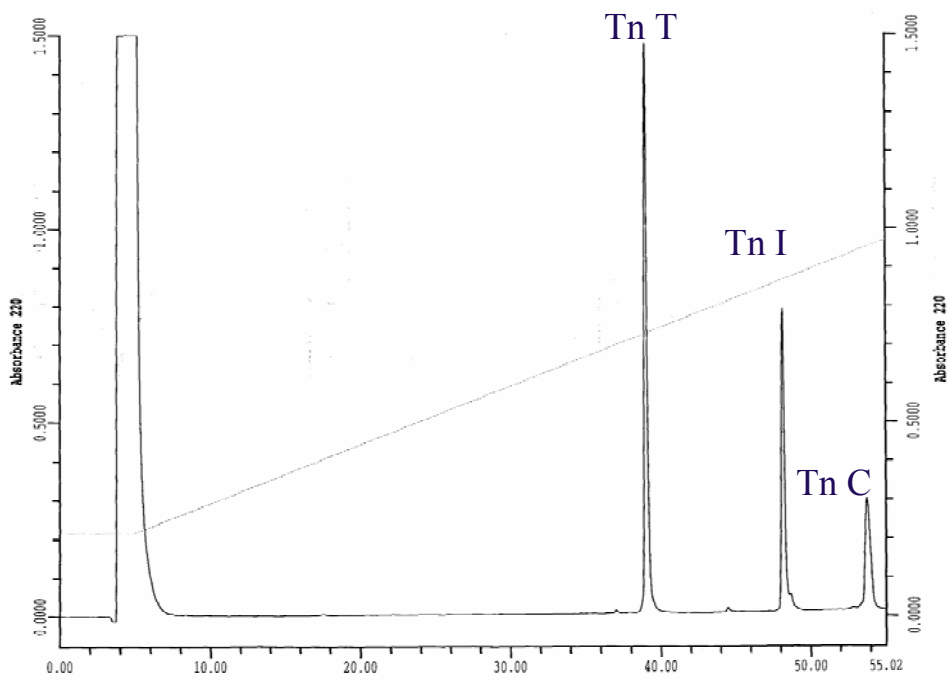


Figure 2.6: Separation of the subunits of rhcTn by reverse phase HPLC. Peak fractions, identified by Edman sequencing and mass spectrometry, were in order of elution TnT, TnI and TnC.

MA) using the standard solvent system of A=0.1% TFA in water and B=0.075% TFA in acetonitrile. Column effluent was monitored at 220 and 280 nm and revealed 3 distinct peaks (Fig. 2.6). The peak fractions, containing protein that later was identified as TnT, TnI and TnC, were collected manually. Collected fractions were concentrated in preparation for Edman sequencing and mass spectrometry.

N-terminal sequencing was performed to verify amino acid sequence of all three rhcTn subunits. Approximately 20% of each RP-HPLC purified peak was loaded onto a biobrene-treated glass fiber filter and subjected to 15 cycles of Edman degradation on a Procise 492 cLC (Applied Biosystems, Foster City, CA) using standard sequencing methods. FASTA analysis of each sequence identified the first RP peak as hcTnT, the second as hcTnI, and the third as hcTnC.

MALDI/TOF mass spectrometry (MS) was performed on a Bruker Biflex III mass spectrometer (Bruker Daltonics, Billerica, MA) equipped with a nitrogen laser (337 nm). Bruker software programs XACQ and XMASS were used for instrument control, data acquisition and data analysis. RP-HPLC purified rhcTnT, rhcTnI, and rhcTnC were diluted 1:5 in sinapinic acid (10 mg/ml in 50% acetonitrile/0.1% TFA, Sigma) and 1µl of each spotted onto the MALDI target. Approximately 200 laser shots were accumulated per sample.

In addition to the wild type, mutations from clinical data were generated by PCR using QuikChange XL Site-Directed Mutagenesis system (Stratagene). Mutations incorporated into the hcTn complex include mutations in TnI, TnI K206Q and TnI R145G, and one mutation in TnT, TnT R278C. In addition, we generated a double mutant by incorporating both TnI R145G and TnT R278C into the hcTn complex. The reactions were carried out according to the manufacturer's instruction with the template of α Tm/pMal-c2 plasmids and the following pairs or primers:

pTnTR278Cf: 5'-GAAAGTCTCCAAGACCTCGGGAAGGCTAAAGTCACCGGGC-3'

pTnTR278Cr: 5'-GCCCGGTGACTTTAGCCTTCCCGCAGGTCCTTGGAGACTTTC-3'

pTnIR145Gf: 5'-GCGGCCACCCCTGGGGAGAGTGAGGATCTCTGCAG-3'

pTnIR145Gr: 5'-CTGCAGAGATCCTCACTCTCCCGAGGGTGGGCCGC-3'

pTnIK206Qf: 5'-GCACTGAGTGGAATGGAGGGCCGCAAGCAAAAAGTTTGAGAGC-3'

pTnIK206Qr: 5'-GCTCTCAAAACTTTTGCTTGCGGCCCTCCATTCCACTCAGTGC-3'

Plasmids extracted from each of the transformed mutants were sequenced with primers strategically designed to cover the pET 41a+ hcTn expression plasmid and to confirm if the desired sequence changes were successful and that no spontaneous mutations occurred. Expression of the hcTn mutants was performed as described for the wild type. The purity of each of the hcTn mutants was determined by coomassie-stained Tricine-SDS PAGE (Fig. 2.7). Gels were imaged using a Kodak EDAS 290 digital imaging system and quantified with Kodak 1D Image Analysis Software.

2.2 In vitro Motility Assays.

2.2.1 Solutions.

In vitro motility assays for measuring the speed of fluorescently labeled filamentous actin (F-actin) motion over HMM-coated surfaces were conducted essentially as described [33, 75, 77]. Reagent solutions were made in ATP-free actin buffer (AB: 25 mM imidazole (pH 7.4), 25 mM KCl, 4 mM MgCl₂, and 1 mM EGTA).

The motility buffer (MB) contained 10 mM EGTA and 20 mM MOPS. Glucose (3 mg/ml), 0.1 mg/ml glucose oxidase, 0.018 mg/ml catalase (Boeringher-Mannheim) and 40 mM DTT were added to minimize photo-oxidation and photo-bleaching [77]. Concentrations of Ca²⁺, Mg²⁺, Na⁺, K⁺, Tris⁺, and acetate were determined [84, 85], taking into account known metal ion binding constants and their enthalpies to obtain an ionic strength of 0.085 M, pH 7, pMg 3, [K⁺] = 50 mM, [Na⁺] = 15 mM, and a pCa of either 5 or 9. Methylcellulose (0.3%), dialyzed against sodium azide (0.02%), was added to MB to prevent F-actin diffusion away from the assay surface [11, 12, 69, 77]. Solutions for assays with reconstituted thin filaments were the same as for unregulated actin, except for the last two solutions: the AB buffer applied to the flow cell before the motility buffer contained either native or recombinant hcTn and either α Tm or β Tm, and was incubated for three minutes before infusing MB containing the same concentrations of hcTn and Tm. The minimum equimolar concentrations of hcTn and Tm added

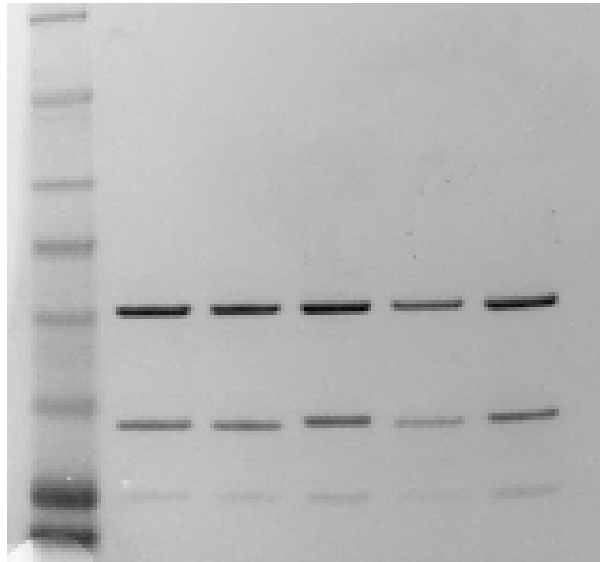


Figure 2.7: SDS-PAGE analysis of representative protein preparations for rhcTn WT and mutants used in this study. Gel was 4-12% polyacrylamide gradient (Invitrogen) and was stained with Simple Blue (Invitrogen). Lane 1: MW marker (Invitrogen See Blue Plus 2). Lane 2: rhcTn WT. Lane 3: rhcTn mutant TnI K206Q. Lane 4: rhcTn mutant TnI R145G. Lane 5: rhcTn mutant TnT R278C. Lane 6: rhcTn mutant TnI R145G·TnT R278C.

Table 2.1: Metabolite concentrations in motility buffers.

	Condition				
	Enzyme-free ¹	Control	High ADP	High Pi	Low ATP
[ATP]	2 mM	2 mM	2 mM	2 mM	0.2 mM
Sucrose phosphorylase	-	5.3 µg/ml	5.3 µg/ml	-	5.3 µg/ml
Sucrose	-	10 mM	10 mM	10 mM	10 mM
[Pi]	~10 µM	~1 µM	~1 µM	4 mM	~1 µM
Creatine Kinase (CK)	-	0.1 mg/ml	0.1 mg/ml	0.1 mg/ml	0.1 mg/ml
Creatine (Cr)	-	30 µM	15 mM	30 µM	12 µM
Creatine phosphate (CP)	-	1 mM	1 mM	1 mM	1 mM
[ADP]	~10 µM	0.42-0.57 µM	213-284 µM	0.42-0.57 µM	~0.02 µM

Values for [Pi], [ADP] and [ATP] represent final concentrations. [ADP] estimates in columns 3 – 6 are based on the equilibrium constant (K_{eq}) for the reaction $ATP + Cr \leftrightarrow ADP + CP$, and are given in columns 3 – 5 with lowest and highest value corresponding to the lowest (27°C) and highest (42°C) temperatures employed, respectively. Values for [Pi] in columns 3 – 6 are estimated using $K_{eq} = 0.06$ for the reaction $sucrose + Pi \leftrightarrow \alpha\text{-D-glucose-1-phosphate} + \text{D-fructose}$ [86, 87]. Estimates of [ADP] in column 2 were based on Chase and Kushmerick [88].
¹Motility buffer employed for the data illustrated in Figs. 3.2—3.10 and 3.15—3.19 did not include sucrose phosphorylase and creatine kinase.

to AB and MB to obtain well regulated filaments were determined by titrations and applying the following criteria: filament gliding had to be inhibited at pCa 9 and motility had to be fast and uniform at pCa 5 and standard temperature of 30°C [12]. To conduct the in vitro motility experiments with varying metabolite concentrations, sucrose phosphorylase and sucrose were added to reduce P_i [86], while sucrose phosphorylase was omitted and acetate partially replaced by P_i to achieve the high P_i condition (Table 2.1); contaminating ADP was removed by addition of creatine phosphate (CP) and creatine kinase (CK), while creatine (Cr) was added with CP and CK to achieve the high ADP condition (Table 2.1) [88].

2.2.2 Flow Cell Preparation.

To prepare flow cells for motility assays, #1 glass coverslips were coated with a thin layer of 0.1% nitrocellulose (NC) in amyl acetate and allowed to dry. Treated coverslips were then mounted on microscope slides with #1½ glass spacers held in place by vacuum grease. Solutions for assays with unregulated actin were infused into the flow cell at room temperature as described [11, 75]. Rabbit HMM (typically 0.25 mg/ml, although [HMM] was reduced in some experiments to vary HMM density on assay surfaces) was incubated in the flow cell for one minute, followed by 0.5 mg/ml BSA for one minute to block nonspecific protein binding. Subsequently the flow cell was flushed with AB to remove unbound BSA. Unlabeled F-actin (0.05 mg/ml, sheared by multiple passages through a 23 gauge needle) was infused into the chamber for one minute, and then the excess was washed out. ATP was infused into the flow cell, and then excess ATP and dissociated unlabeled F-actin were washed out. These steps of unlabelled actin and ATP washes effectively block ATP-insensitive myosin heads [77]. RhPh-labeled F-actin (0.33 µg/ml) was incubated in the flow cell for one minute, and unbound labeled actin was washed out of the flow cell. MB was then added, and the RhPh-labeled actin was imaged by video fluorescence microscopy.

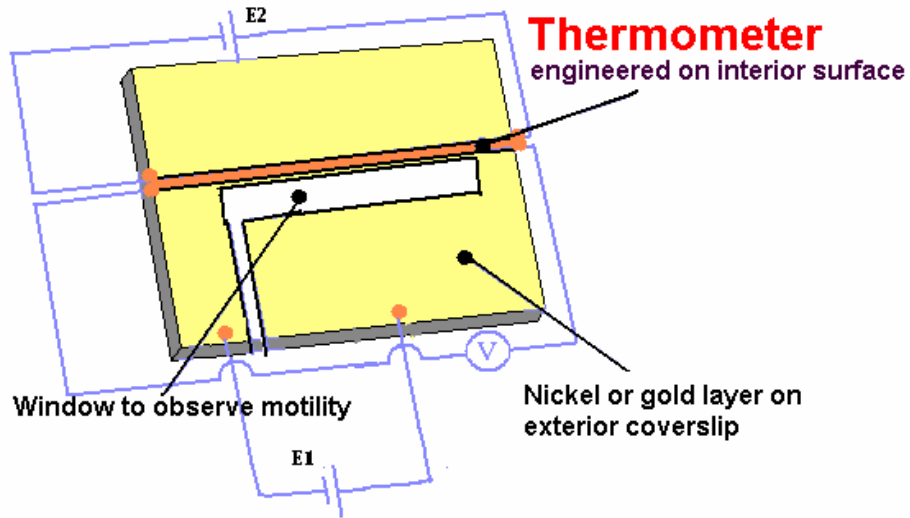
Steady-state temperature of flow cells was maintained by circulating temperature-controlled (better than $\pm 1.0^\circ\text{C}$) water through a copper coil wrapped around the microscope objective [75]. Temperature inside the flow cell was calibrated using a thermistor (< 1 mm; model T10K30, Quest Scientific). Steady-state temperature experiments were conducted at 27°C, 30°C, 32°C, 37°C, or 42°C.

2.2.3 Temperature Transients.

Temperature transient data were collected as previously described [33]. Flow cells were modified by fabricating a heater and a thermometer onto opposite sides of the glass coverslip (Figure 2.8A). Thin Au film heaters, 80 – 100 nm thick, were deposited by thermal evaporation and photolithographically patterned on the outer side of the coverslip by lift-off. Photolithography and lift-off were also employed in the fabrication of gold resistive thermometers that were thermally evaporated on the underside of the coverslip in the form of 10 μm wide and 80 nm thick stripes. The heater and thermometer were independently biased by two DC source meters (Keithley, MODEL 2400) that also measured the voltage drop over the thermometer stripe in a four-probe configuration. Experimental control and data acquisition were accomplished with a custom LabVIEW program. The thermometers were electrically insulated with GE Varnish and calibrated over the temperature range 10°C to 70°C. Resistance varied linearly with temperature as expected (Figure 2.8B). To minimize temperature gradients, the thermoelectric heater covered most of the flow cell except for a small central observation window, with the thermometer stripe located $\sim 500 \mu\text{m}$ from the window's edge. The magnitude of the current to heat the flow cell was typically 0.8 – 0.9 A (corresponding to a density of $\sim 2 \times 10^5 \text{ A/cm}^2$), after which it was turned off and the system was allowed to cool for the same period of time. The low starting temperature (14 – 18°C) and the cooling process were realized by chilled water flowing through the copper coil wrapped around the microscope objective.

Over the course of this study, the thermo-electric controller was upgraded by engineering multiple thermometer stripes on the surface, allowing measurements of thermal gradients, and allowing easier recycling of the modified coverslip [74]. Electrical insulation with GE Varnish was replaced by covering the entire coverslip, including the heaters by a 100-nm-thick SiO_2 layer that was fabricated by RF sputtering in ATC 1800-F sputtering system (AJA International, Inc.) using a base pressure 10^{-8} Torr, Ar pressure 3 mTorr, flow rate 30 sccm, forward power 120 W. The SiO_2 layer was then coated with NC (Fig. 2.9A). As opposed to the use of GE Varnish as an insulator, which creates large irregular regions in the flow cell that can not be monitored, the use of SiO_2 insulation allowed viewing of motility in the immediate vicinity of the heater, only restricted by the area of the flow cell directly underneath the heater (Fig 2.9B).

A



B

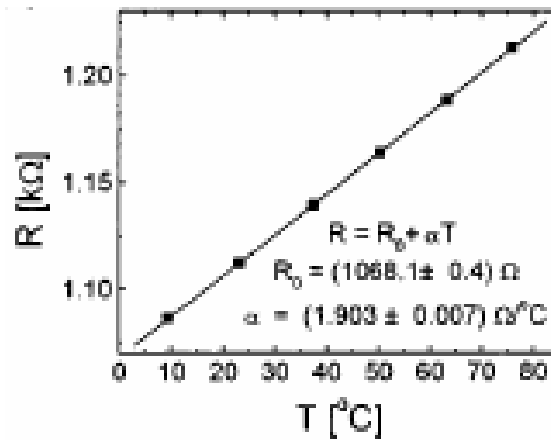


Figure 2.8: Design and calibration of the thermo-electric controller for motility assays. (A) A modified cover slip with lithographically defined heater, covering most of the flow cell except for an observation window (yellow, on the exterior of the cover slip), and the thermometer (orange stripe, on the interior surface) on the same cover slip for temperature dependent measurements of filament sliding speed in motility assays. **(B)** Typical resistance (R) vs temperature (T) characteristic of a thin narrow-stripe gold thermometer (panel A). Sensitivity of the thermometer, $a=dR/dT$, is given in the inset. The figure in panel B was reproduced from Mihajlović et al. [33].

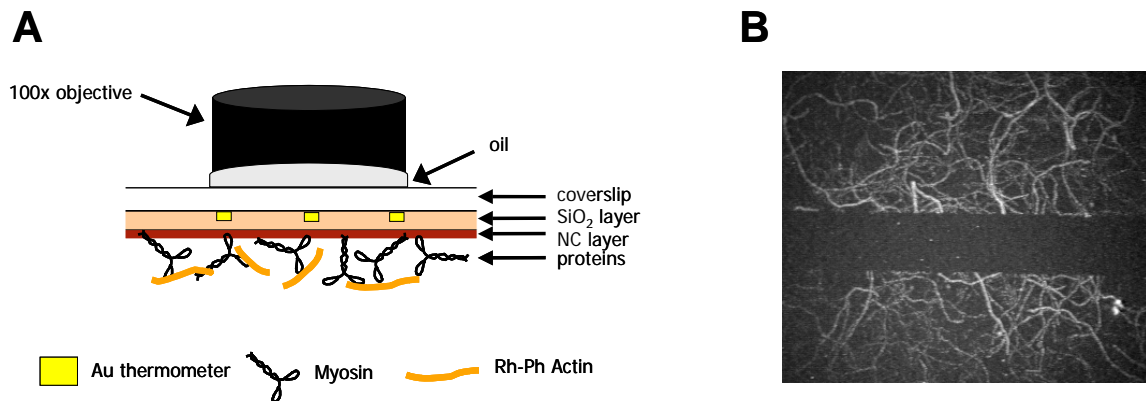


Figure 2.9: (A) Schematic of motility surface of flow cell modified with Au heating elements and electrically insulated with a 100 nm layer of SiO₂ and (B) fluorescence images (30 frames; 5 seconds) of motile F-actin. Images in panel B are stacked to illustrate the presence of an Au heating element which is interposed between the sliding filaments and the microscope objective and thus blocks transmission of rhodamine fluorescence but not motility. Fluorescently labeled actin filaments were propelled by HMM adsorbed to the layer of nitrocellulose on SiO₂. The heating element is evident as a dark region that extends completely across this fluorescence image stack; width of heating element is 10 μ m. Figures reproduced from Grove et al. [33].

2.2.4 Data Acquisition and Analysis.

Fluorescence microscopy was accomplished using a Diastar-Reichert microscope at 100x magnification with Hg lamp illumination. Video images of RPh-labeled F-actin motility were recorded for at least 30 s per field using a VE1000 SIT camera (Dage-MTI, Inc) and a Panasonic AG-7350 video recorder.

Two methods were employed to measure the speed of the sliding filaments:

1. Motility speed was analyzed using MetaMorph software (Universal Imaging) as described previously [33]. Stacks of frames (one stack for each second of recorded temperature transient data or 10 – 12 stacks, each representing 1-3 seconds of recorded data, for each steady state experiment) were created from digitized movies; actin filament paths were visualized by superimposing all the frames of one stack to form a projection and subtracting the image of the first frame. For each stack (Fig. 2.10), 4 – 8 filaments were randomly selected and the distance traveled (d) was estimated by manually measuring the residual contour lines of their respective pathways (Fig. 2.10). Speed was determined as $d/(\Delta t(\#frames - 1))$, where Δt ($\Delta t = 0.0333$ s) is determined by the 30 frames-per-second video recording.
2. Alternatively, 5-6 fields from varying areas on the flow cell were recorded for 30 seconds and subsequently processed using iMovie software as QuickTime files on a Macintosh 2X PowerPC G4 computer with a Miglia video interface (Miglia Technology Ltd, Enfield, UK). RhPh F-actin sliding speed distributions were analyzed by custom motion analysis software programs (designed by Thomas Asbury and P. Bryant Chase). Individual filament speed was measured by edge-detecting software, generating a data file for each Quick Time file containing the Cartesian coordinates of the trailing end, the leading end, and the centroids of each filament for each frame (raw data). The mean speed for all filament paths was calculated from the raw data files after either removal of erratic filaments ($SD/average\ speed > 0.3$) or removal of immobile filaments ($speed < 0.5\ \mu\text{m/s}$). [12, 75, 89]. In addition, custom software was written that processes the raw data files and allows variable selection criteria, facilitating data analysis with different myosin isoforms having different maximum speeds.

2.2.5 HMM Density (ρ).

The density of competent HMM on the NC-coated surface (ρ) was determined as a function of the concentration of HMM introduced into the flow cells by measuring K-EDTA

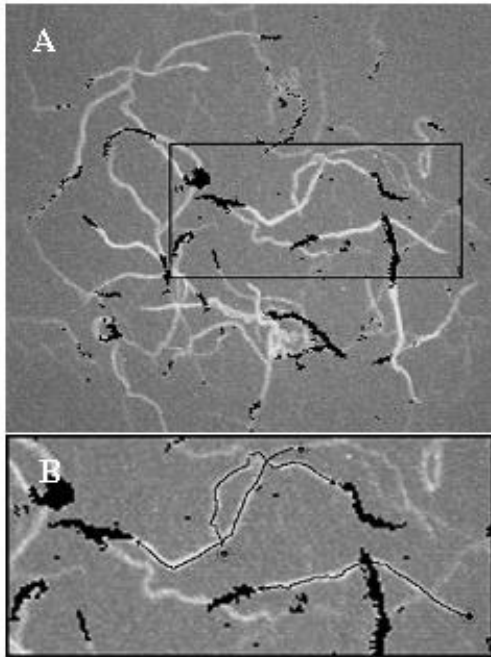


Figure 2.10: Analysis of actin motility. (A) Superposition of 90 sequential video frames from one representative recorded fluorescence microscopy field. White traces indicate the paths of RhPh-labeled actin filaments over 3 s. Actin filaments in the last frame are indicated in black. (B) Rectangular area from panel A magnified to illustrate measurement of the distance traveled by the trailing ends of three actin filaments. The trailing end of each actin filament is marked with a dot in the 1st frame and with an arrowhead in the 90th frame. Each path contour begins at the dot and proceeds to the arrowhead. Hence the arrowheads also represent the direction of filament sliding.

